Initiator-dependent kinetics of lyotropic liquid crystal-templated thermal polymerization

Younes Saadat,[1] Kyungtae Kim,[2] Reza Foudazi [1*]

[1] *Department of Chemical and Materials Engineering, New Mexico State University, Las Cruces, NM 88003, USA*

[2] *Materials Physics and Applications Division, Center for Integrated Nanotechnologies, Los Alamos National Laboratory, Los Alamos, NM 87545, USA*

Abstract

In this study, we examine the polymerization kinetics with different thermal initiators in lamellar and hexagonal lyotropic liquid crystal (LLC) structures directed by Pluronic L64. Ammonium persulfate is used to initiate the polymerization from the water phase, whereas azobisisobutyronitrile and benzoyl peroxide are employed to commence the reaction through the monomer phase. While the mesophase structure remains intact for all the initiation systems, the kinetics of polymerization and conversion vary significantly. The obtained differential scanning calorimetry (DSC) results reveal that, under same conditions, initiation from water (IFW) system results in enhanced reaction rates as well as higher monomer conversions compared to initiation from oil (IFO) one. Higher termination rate in LLC nanoconfinements induces lower reaction rates in IFO system. Moreover, our work on different LLC structures show that the effect of nanoconfinement on polymerization rate can be minimized through IFW. Chemorheology not only confirms the results obtained from DSC, but also shows that, in similar monomer conversions, the polymers obtained from IFW system exhibit an improved mechanical properties over the samples produced though IFO process.

Keywords: *Lyotropic liquid crystal templating, Mesophase, Thermal polymerization, Self-assembly*

[*] *Corresponding author. MSC 3805, P. O. Box 30001, Las Cruces, NM, 88003-3805, USA, Email: rfoudazi@nmsu.edu.*

Introduction

Nanostructured materials have attracted the attention of scientific communities as well as industries since they have application in a plethora of technical fields such as drug delivery systems,[1,2] membranes,[3,4] and energy storage devices.[5] Precise control of the nanostructure, process-ability, and chemical functionality are important factors which should be considered in designing such materials to fulfil the requirement of each application.[6]

Amongst a variety of available methods for fabrication of nanostructured components, molecular self-assembly has received a great deal of attention thanks to its high performance in the production of precisely designed structures in nano-scale.[3,6–13] Self-assembly of amphiphilic molecules is one of the best examples in this field since it can result in liquid crystals (LCs) with different nanostructures, which simultaneously have the fluidity of liquids and anisotropy of solids. LCs of organic compounds are obtained either in the molten state (thermotropic LCs), or in the presence of a solvent as in lyotropic LCs (LLCs).[14] Although LLCs offer a variety of nanostructures (e.g., lamellar, hexagonal, and bicontinuous cubic), they suffer poor mechanical properties and thermal stability.[15–17] Therefore, applicability of such interesting structured materials in many applications is not practical. Alternatively, LLCs can be used as template to polymerize organic species, resulting in nanostructured polymers.[17–20] Such templating approach is performed in two main ways: synergistic and transcriptive templating. In synergistic templating, cured template is obtained though the polymerization of reactive surfactant that forms the template. In the case of transcriptive templating, one-to-one replica is fabricated through the polymerization of reactive species confined in the LLC nanostructure.[15,21]

The most important challenge in LLC templating is preservation of the nanostructure during polymerization, which can be altered due to the phase-separation/inversion.[22,23] There have been several efforts to address this issue. Cross-linking the polymer chains[10,11,20,24,25] and using block copolymer surfactants[26–29] are the main approaches to overcome this problem. Cross-linking makes the polymer network kinetically trapped and block copolymer amphiphiles induce a kinetically slow phase-separation/inversion.[30] Additionally, the rate of polymerization is a complementary factor affecting nanostructure preservation during LLC templating. The higher the polymerization rate, the higher will be the chance of the structure retention. Furthermore, the polymerization kinetics can be used as a tool to predict any probable structural changes during templating since any discontinuities in the profile of the reaction rate can be a sign of structural alterations.[15]

Due to the importance of polymerization kinetics during LLC templating, Guymon and coworkers studied the kinetics of photopolymerization in LLCs. They have examined the photopolymerization kinetics of different reactive species (e.g., polymerizable surfactants [31–33] and monomers[26,34,43,35–42]) in a wide variety of LLC nanostructures. Their results have shown that the location of polymerizable group on the reactive amphiphile and the length of lipophilic chain are

the main parameters that control the reaction kinetics in synergistic templating.[31–33,44] Both of these parameters affect the polymerization rate via changing the local double bond concentration. The higher the local double bond content, the higher is the polymerization rate. They have also studied the photopolymerization kinetics in transcriptive templating.[26,34,43,35–42]Their observations show that the monomer and photoinitiator polarity are the key parameters in the polymerization kinetics.[15] The polymerization rate increases with a change in LLC structure from normal micellar to lamellar when hydrophilic monomers are used. They attributed this observation to the enhanced propagating rate due to the higher local monomer concentration in polar domain and suppressed termination rate because of the limited mobility of propagating chains, which are the consequences of the monomer partitioning.[36,39–42,45,46] In contrast, hydrophobic monomers show the opposite behavior, meaning that the polymerization rate decreases with a change in LLC structure from micellar to lamellar.[26,34–38] Based on the reported results, higher local concentration of the photoinitiator can promote the recombination reactions of free radicals due to the cage effect, resulting in lower polymerization rate. Accordingly, while hydrophobic photoinitiators show higher reaction rate when the LLC structure changes from normal micellar to lamellar, the opposite trend is seen for hydrophilic species.[15,35–37]

Even though photopolymerization is frequently used in LLC templating, thermal polymerization is an alternative approach that is more favorable for industrial scale synthesis of polymers. However, there are few systematic works on evaluating the thermal polymerization in LLC templating. DePierro *et al.* have reported that it is challenging to preserve the LLC structure during thermal polymerization of acrylamide, possibly because of slow reaction rate.[45] However, Qavi and coworkers have shown the possibility to retain the structure (e.g., hexagonal and lamellar) when the thermal polymerization is used.[24,30] They have also found that the reaction is slower in nanoconfinements with lower domain size of polymerizing phase and attributed this observation to higher probability of termination reaction.[30]

In this study, we use poly(ethylene oxide)-poly(propylene oxide)-poly(ethylene oxide) (PEO-PPO-PEO) triblock copolymers (also known as Pluronics or Poloxamers) as the surfactant in combination with water and oil phases to create inverse hexagonal (H_2) and lamellar (L_α) structures. The oil phase contains n-butyl acrylate (nBA) as monomer and ethylene glycol dimethacrylate (EGDMA) as cross-linker. Two types of thermal initiation system are used to polymerize the oil phase: initiation from water (IFW) by using ammonium persulfate (APS) and initiation from oil (IFO) by employing azobisisobutyronitrile (AIBN) or benzoyl peroxide (BPO). Despite the fact that monomer and crosslinker form the oil phase, we show that the polymerization rate is much faster in the case of IFW compared to IFO. Faster polymerization rate has already been reported for APS over AIBN in an inverse emulsion polymerization of acrylamide.[47] In such polymerization system, free radicals generated by oil-soluble AIBN diffuse into hydrophilic polymer particles as monomer-rich loci, resulting in slower reaction rate. In contrast, even though free radicals of water-soluble APS migrate into the monomer-rich oil phase in the current study, the reaction is still faster for APS compared to AIBN. Furthermore, our experiments reveal that in

similar monomer conversions, the templated product using IFW system exhibits enhanced mechanical properties than the samples obtained from IFO approach. Both observations make the current study unique in terms of the effect of initiation system on polymerization kinetics as well as the mechanical properties of final products. We also study the effect of initiator concentration and the temperature on the polymerization kinetics.

Experimental

Materials. Pluronic L64 (PEO_{13}-PPO_{30}-PEO_{13}) with the polydispersity index of 1.1[48] was kindly provided by BASF. nBA, EGDMA, APS, AIBN and BPO were purchased from Sigma-Aldrich and used as received. Deionized water (0.055 μS/cm, EMD Millipore Direct-Q3) was used as the aqueous phase. The reaction scheme and chemical structures of the employed materials are shown in Fig. 1a-e.

Preparation of Mesophase Samples. Pluronic/water/oil weight ratios of 50/35/15 and 55/15/30 were used to produce lamellar and hexagonal structures, respectively.[24] To prepare the mesophases, the components were mixed using centrifugation at 10000 rpm for 10 min. The centrifugation was repeated in alternating directions until a transparent gel was obtained. EGDMA concentration in the oil phase was adjusted on 30 wt% with respect to nBA content. For all of the initiators, 5 mol% concentration was used with respect to the total monomer content (nBA + EGDMA). To incorporate the initiators, APS was dissolved in water and the oil soluble initiators were dissolved in the monomer phase before mixing and centrifugation. To evaluate the effect of combining IFO and IFW systems on the polymerization kinetics, some samples were prepared with 2.5 mol% APS in water phase and 2.5 mol% AIBN or BPO in oil phase.

Structural Characterization. A cross-polarized light microscope (model BX60, Olympus) was used to characterize the structure of mesophases before and after the polymerization to assess any structural changes during reaction. A small amount of non-polymerized, mesophase sample was placed on a glass slide and covered with a glass cover slip. Cross-polarized images of samples were taken using a microscope-mounted digital camera. Small angle X-ray scattering (SAXS) was employed to further characterize the structure of LLCs before and after the reaction. The mesophase samples were loaded into quartz capillaries with a nominal diameter of 1.5 mm (Charles Supper Company, Natick, MA) by centrifugation, followed by sealing with critoseal and epoxy glue. The samples were then cured in the capillaries at 65 °C for 24 hours to study the structure after the polymerization. A Bruker Nanostar X-ray scattering system equipped with a monochromated Cu Kα radiation source was used for SAXS measurement. One dimensional (1D) scattering profiles were generated via azimuthal integration of the two-dimensional (2D) scattering patterns.

Polymerization Kinetics. Isothermal differential scanning calorimetry (DSC) was performed using

Q2000 (TA Instruments, New Castle, DE). Approximately 10 mg of mesophased sample was placed in a Tzero aluminum pan and sealed with a Tzero hermetic lid. The polymerization kinetics at 65 °C (± 0.1 °C) was studied under nitrogen atmosphere. To evaluate the effect of the reaction temperature on the reaction kinetics, some experiments were also performed at 55 and 75 °C. To determine the rate of polymerization (normalized to the total reactive concentration), the procedure developed by Guymon et al. was employed.[34,36,38,43] Having the heat flow, $Q(t)$, the polymerization rate, R_p, was calculated using Eq. (1):[30]

$$\frac{R_p(t)}{[M]_0} = Q(t)\left[\left(\frac{M}{n\Delta H_p m}\right)_{monomer} + \left(\frac{M}{n\Delta H_p m}\right)_{crosslinker}\right] \quad (1)$$

where M, $[M]_0$, ΔH_p, n, and m are monomer molar mass, initial monomer concentration, theoretical reaction enthalpy (86,200 J/mol for acrylates and 56,000 J/mol for methacrylates),[49] functionality, and the total mass of corresponding species (i.e., monomer or crosslinker), respectively.[43,50] The degree of monomer conversion was calculated by integrating the area under the $R_p(t)/[M]_0$ versus time curve since $R_p(t)/[M]_0 = -\frac{dp}{dt}$ with p being the double bond conversion.[46] Schematic of the polymerization process in different LLC structures is shown in Fig. 1f.

Chemorheology and Mechanical Properties. A stress-controlled rheometer DHR-3 (TA Instruments, New Castle, DE) was used to study the chemorheology and the mechanical properties of the polymerized samples.[30] A 40 mm sand blasted parallel plate geometry with 1 mm gap was employed in all of the experiments to suppress the wall-slip, which was confirmed to be indeed negligible in uncured and cured mesophases (Fig. S1) in agreement with previous study.[51] A solvent trap filled with deionized water was used to minimize any probable monomers or water loss during the reaction at 65 °C under the rheometer. In the case of chemorheology, the tests were performed in the linear viscoelastic region (0.1% strain, confirmed from amplitude sweep tests). The evolution of dynamic moduli with time at 65 °C was considered for determining the polymerization kinetics.[52] To evaluate the mechanical properties of polymerized LLCs, after curing the sample under rheometer, the temperature was decreased to 25 °C and then dynamic frequency sweep test was carried out in the frequency range of 0.1 to 400 rad/s.

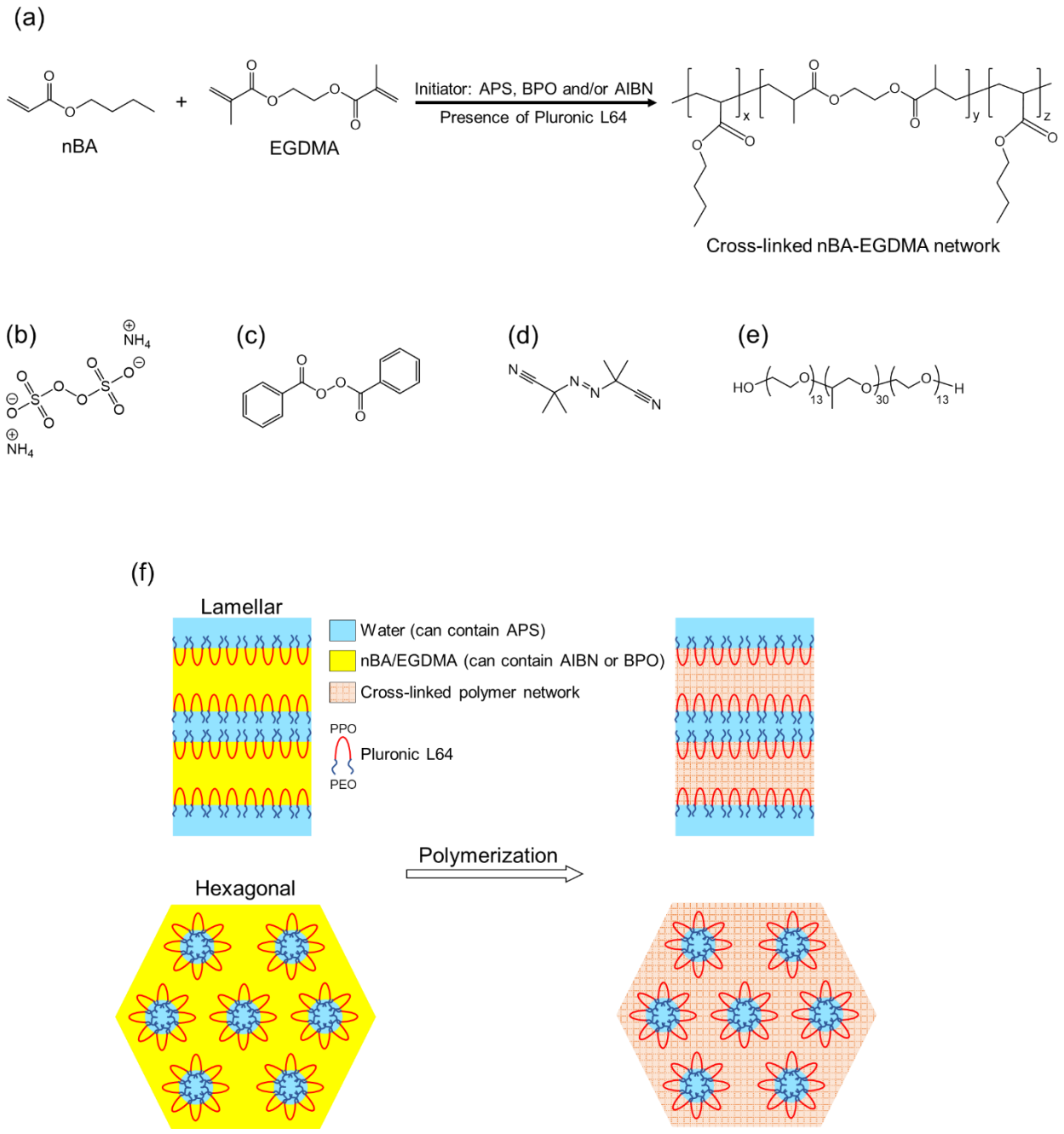

Fig. 1. (a) Monomers and reaction scheme of their polymerization process in this study; (b-e) Chemical structures of initiators and surfactant: (b) APS, (c) BPO, (d) AIBN, and (e) Pluronic L64; (f) Schematic of polymerization process in lamellar and hexagonal structures.

Results and discussions

Cross-polarized light microscopy (CPLM)

We previously showed that Pluronic L64/water/oil systems with weight ratios of 50/35/15 and 55/15/30 have lamellar and hexagonal structures, respectively.[24] To confirm the preservation of these LLC structures after polymerization, Cross-polarized light microscopy studies were carried out on the LLC samples before and after polymerization. The obtained results are shown in Fig. 2. Streaky-oil and fan-like texture is observed for lamellar and hexagonal structures,[24] respectively, before polymerization regardless of the applied initiation system. The absence of extinction (a dark image) in the CPLM photograph of polymerized species indicates that the structure remains birefringent after the polymerization using IFW or IFO systems.

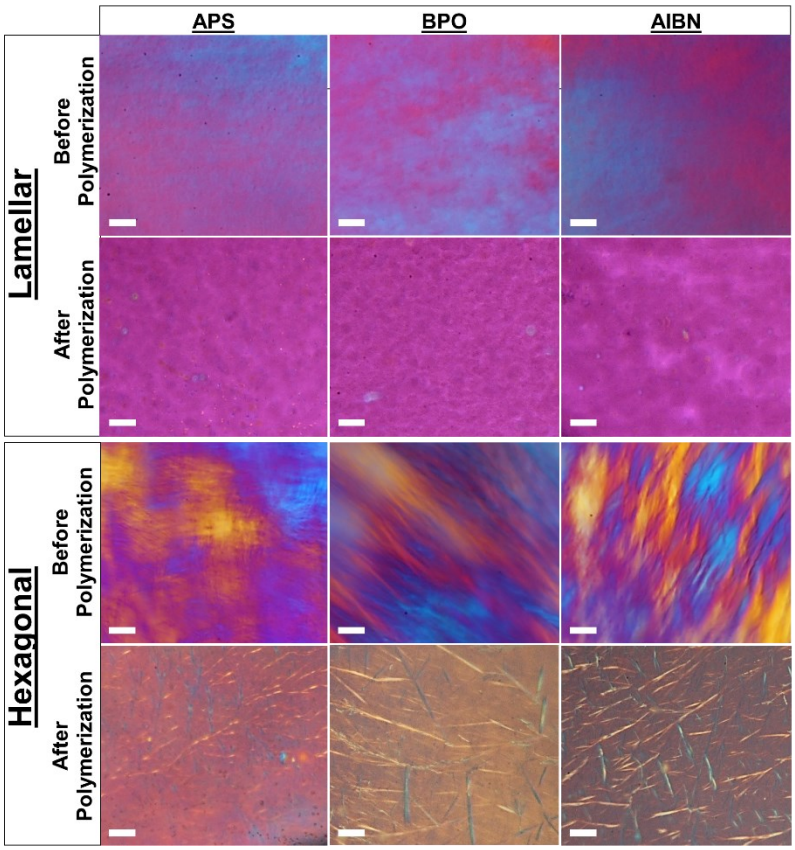

Fig. 2. CPLM images of LLCs with lamellar and hexagonal structures before and after thermal polymerization by IFW and IFO systems. Scale bar: 50µm.

Small Angle X-ray Scattering (SAXS)

To confirm the results of CPLM and study the structure of LLCs quantitatively, we performed

SAXS analysis. The SAXS results for lamellar and hexagonal systems before and after curing with different initiators are shown in Fig. 3. As expected, Bragg peaks with ratios of 1:2 and 1:√3 are observed for lamellar and hexagonal structures, respectively, before polymerization. The peaks with similar ratios are obtained after polymerization via different initiators for both lamellar and hexagonal phases. The only notable point here is the change in positions of the peaks after polymerization which is a sign of change in *d*-spacing of the structures after polymerization. Such structural changes have commonly been reported in the literature for polymerization of LLCs.[12,24,30,53]

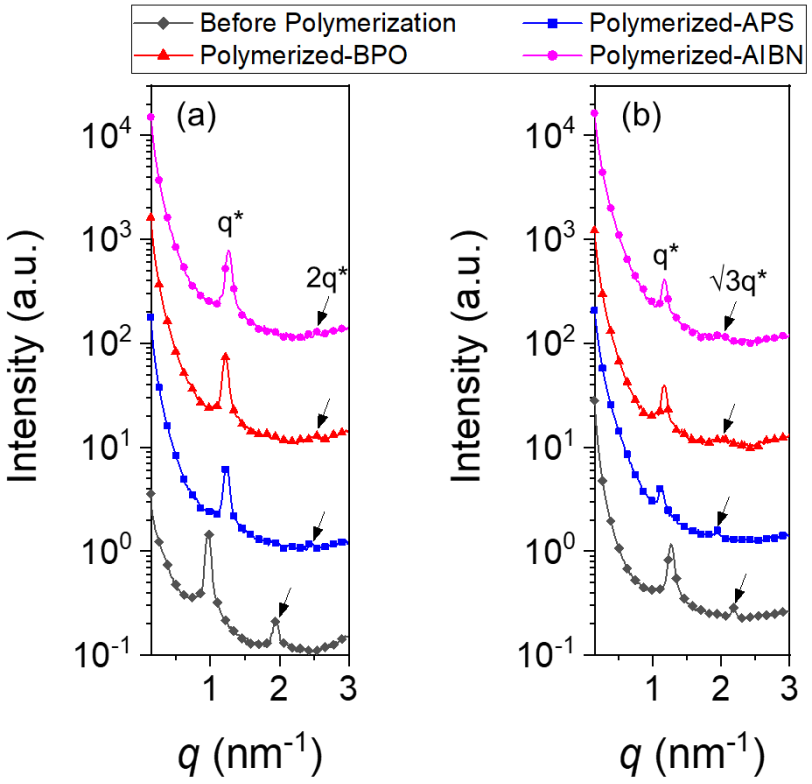

Fig. 3. 1D SAXS data for (a) lamellar and (b) hexagonal phases before and after polymerization with different initiators. The plots are vertically shifted for clarity.

Using the obtained data for the principal scattering vector, q^*, we can calculate the lattice parameter for both structures (see the schematic illustration presented in Fig. 4) using the following equations:

$$d = \frac{2\pi}{q^*} \qquad (2)$$

$$a = \frac{4\pi}{\sqrt{3}\, q^*} \tag{3}$$

where d is the lattice parameter (also known as the lamellar periodicity) for lamellar structure and a is the lattice parameter (equal to the distance between the centers of adjacent cylinders) for hexagonal phase.

The volume fraction of apolar domain, ϕ, was defined as the volume fraction of the monomer phase and PPO block. Additionally, the volume fraction of PEO chains and water was considered as the volume fraction of polar domain, 1- ϕ. Using these parameters, we calculated the size of apolar domain for lamellar (δ) and hexagonal structures (R) using the following equations:[24]

$$\delta = d\phi \tag{4}$$

$$R = a\left[1 - \left(\frac{\sqrt{3}}{\pi}(1-\phi)\right)^{1/2}\right] \tag{5}$$

To evaluate the effect of nanoconfinement on the polymerization kinetics, it is required to calculate the nanoconfinement radius for lamellar ($R_{l,\,max}$) and inverse hexagonal ($R_{h,\,max}$) structures using the following equations:[30]

$$R_{l,\max} = \frac{\phi_{Oil} d}{2} \tag{6}$$

$$R_{h,\max} = a\left[\frac{\sqrt{3}}{4\pi}\left(1 - \phi_{Pluronic} - \phi_{Water}\right)\right]^{\frac{1}{2}} \tag{7}$$

where ϕ_{Oil}, $\phi_{Pluronic}$, ϕ_{Water} are volume fraction of oil, Pluronic, and water, respectively. To calculate the mentioned volume fractions, we followed the assumptions and procedures proposed earlier.[24] Briefly, by considering the complete segregation of the water, PEO, PPO, and monomer phases and thus using their bulk density, the volume fractions are calculated. The radius of gyration (R_g) for Pluronic P85 (PEO_{25}-PPO_{40}-PEO_{25}) is 1.7 nm.[55] Pluronic P85 has a higher polymerization degree than Pluronic L64, thus, the latter has even smaller R_g. Therefore, as discussed by Qavi et al.,[54] there is hardly any bridging between polar/apolar domains by Pluronic chains in this system.

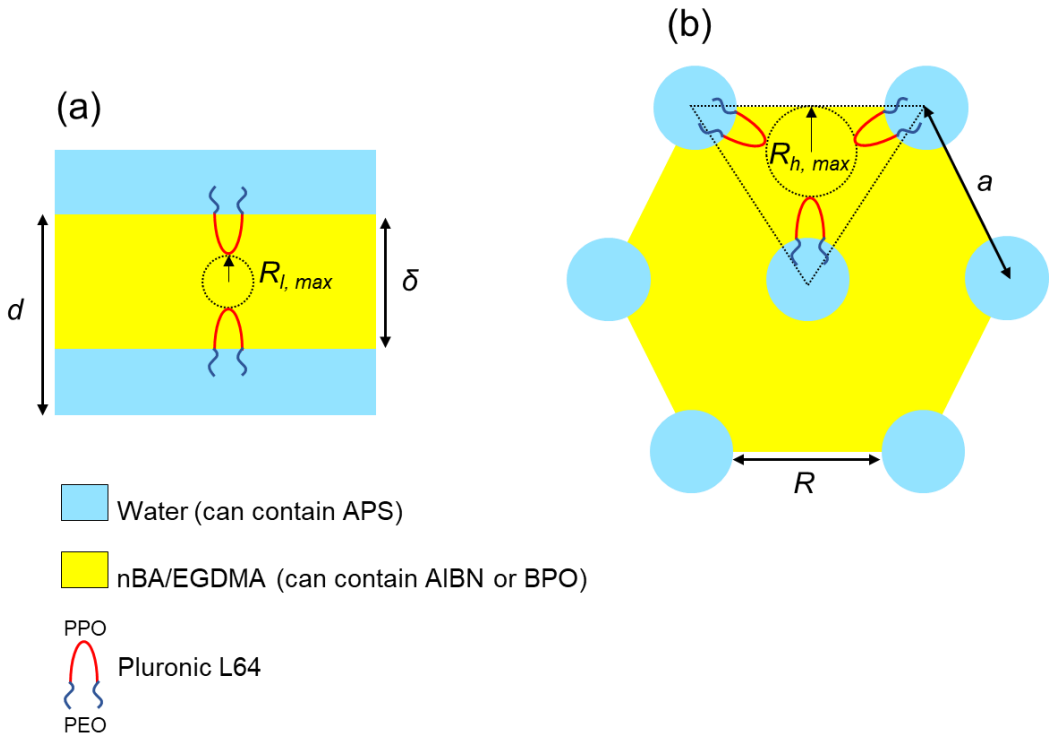

Fig. 4. Schematic illustration of (a) lamellar and (b) hexagonal phases with structural parameters that can be obtained from SAXS analysis. The nBA/EDGMA region is where polymerization/crosslinking occurs.

Table 1 shows the results of the aforementioned calculations. The confinement size almost remains unchanged regardless of the employed initiation system. Additionally, the confinement size is bigger for hexagonal structure compared to lamellar one, which can significantly affect the polymerization kinetics, as previously reported in the literature[30] and will be discussed in the following sections. It is also noteworthy that the lattice parameter as well as apolar domain size change upon polymerization for both structures, which is a common phenomenon in polymerization of LLCs that happens due to the formation of polymer network and thus the competition between thermodynamics and kinetics.[12] In terms of thermodynamics, the thermodynamic penalty of mixing increases by increasing the molecular weight of the oil phase. Such increase in the thermodynamic penalty coupled with the change in surface energy of the polymerizing phase can induce phase separation, resulting in the domain size increase. On the other hand, the density increases due to the formation of polymer network (shrinkage of the polymerizing phase) which can result in smaller domain sizes. Due to the suppression of the chains mobility by the cross-linking, the phase separation and thus complete loss of nanostructure is avoided, but yet the domain size is controlled by the competition between demixing and shrinkage.[24,56]

Table 1. Calculated parameters for different LLC structures before and after polymerization.

Sample	LLC structure	d or a (nm)	ϕ	ϕ_{Oil}	$\phi_{Pluronic}$	ϕ_{Water}	δ or R (nm)	Confinement size (nm)
Unpolymerized	L_α	6.40	0.46	0.16	0.49	0.36	2.95	~0.5
	H_2	5.75	0.64	0.31	0.54	0.15	3.19	~1.2
APS-initiated	L_α	5.06	0.46	0.16	0.49	0.36	2.33	~0.4
	H_2	6.47	0.64	0.31	0.54	0.15	3.59	~1.3
AIBN-initiated	L_α	4.98	0.46	0.16	0.49	0.36	2.29	~0.4
	H_2	6.25	0.64	0.31	0.54	0.15	3.46	~1.3
BPO-initiated	L_α	5.15	0.46	0.16	0.49	0.36	2.37	~0.4
	H_2	6.25	0.64	0.31	0.54	0.15	3.46	~1.3

Thermal Polymerization Kinetics

DSC was used to study the thermal polymerization kinetics in LLC nanoconfinements dependent on initiators. The calculated normalized polymerization rate and overall monomer conversion for LLC structures are shown in Fig. 5. It is noteworthy that for all of the initiation systems, the absence of any fluctuation and/or discontinuities in DSC results (see Fig. S2 for typical raw DSC data) confirms that no structural changes happen during polymerization of LLCs.[15] This conclusion agrees with SAXS results, proving the retention of structure during polymerization of studied samples.

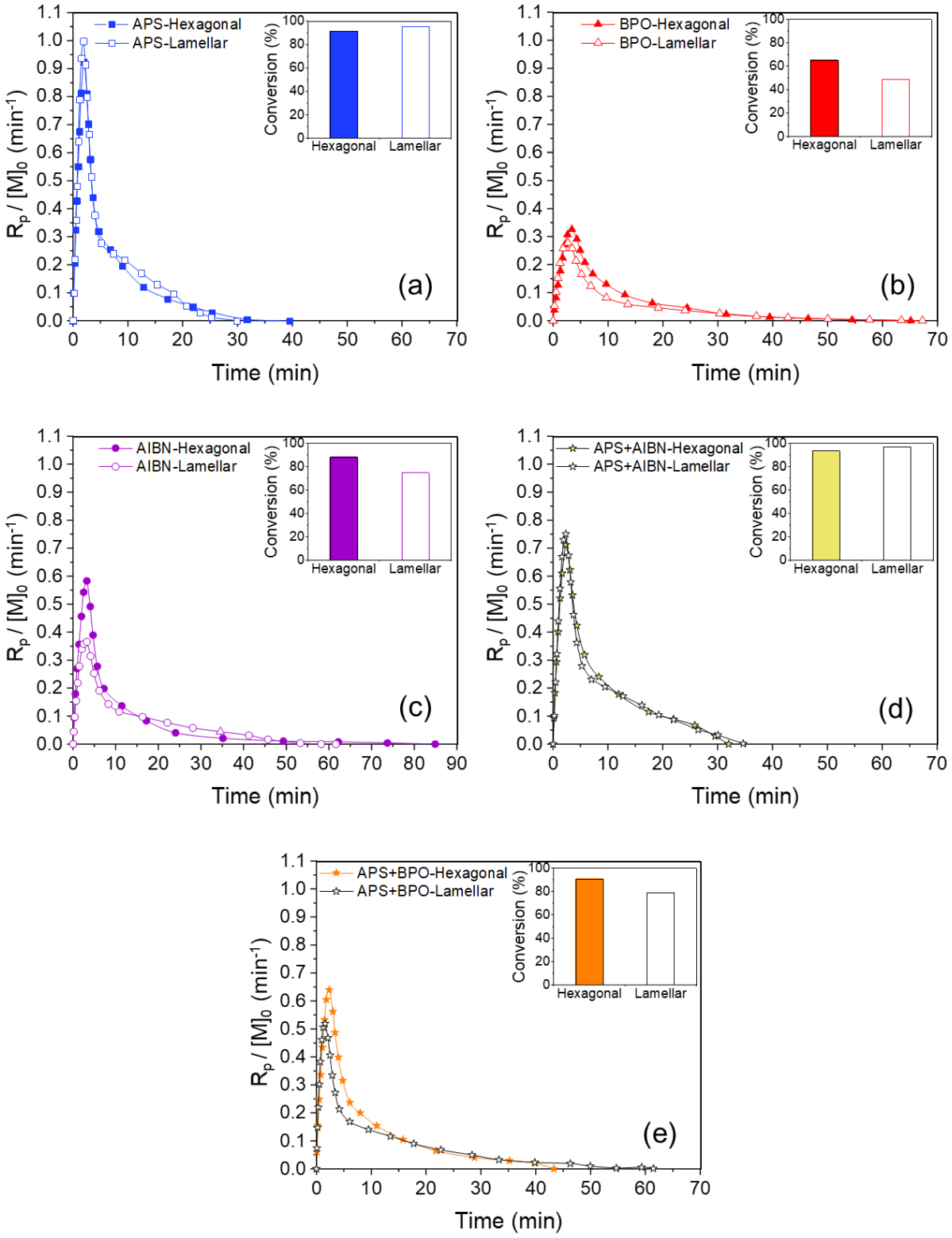

Fig. 5. Normalized polymerization rate versus time and overall monomer conversion obtained from thermal polymerization in hexagonal and lamellar structures using different initiation systems: (a) APS, (b) BPO, (c) AIBN, (d) APS+AIBN and (e) APS+BPO. For all samples, the total initiator concentration of 5 mol% was used with respect to the total monomer content.

Unexpectedly, APS-initiated thermal polymerization (IFW) shows much faster polymerization rate compared to the IFO reactions initiated by AIBN and BPO. The maximum polymerization rate for IFW system is ~2.5-3 times higher than for IFO ones. Furthermore, the overall monomer conversion is more than 90% for IFW, whereas less than 75% conversion is achieved with IFO approach. One might argue that such difference is due to the different free radical concentrations generated by different initiators. To examine this hypothesis, we calculated and plotted the theoretical concentration of free radicals (normalized with the initiator efficiency) produced by different thermal initiators over time at 55, 65, and 75 °C and initial initiator concentration of 5 mol% with respect to the total monomer content. The calculation and results are presented in the Supporting Information (SI text and Fig. S3). AIBN has the highest free radical generation capability and the concentration of the free radicals generated by APS is in between of AIBN and BPO. Therefore, the free radical concentration is not the major factor determining the reaction rates for different initiation systems.

To further evaluate IFW and IFO, we polymerized the oil phase in the same structure using a combination of IFW and IFO systems (APS/AIBN and APS/BPO). We used 2.5 mol% of each initiator to adjust the total initiator content to 5 mol% with respect to the total monomer concentration. The acquired results show that the reaction kinetics for IFW+IFO fits in between of IFW and IFO systems. Additionally, the maximum polymerization rate is almost doubled for both AIBN and BPO when combined with APS. Furthermore, the overall monomer conversion enhanced from ~75% to ~97% and from ~50% to ~80% for AIBN+APS and BPO+APS, respectively. These results become interesting when we compare the free radical concentration trend for the mixed initiation systems with those for separate initiators (see Fig. S3). The concentration of active sites decreases when we combine 2.5 mol% APS with 2.5 mol% AIBN, but the reaction rate as well as monomer conversion increases compared to 5 mol% AIBN alone. In contrast, the free radical content of 2.5 mol% BPO combined with 2.5 mol% APS is higher than that of 5 mol% BPO and still the polymerization rate and monomer conversion improve. Based on these observations, one may suggest that there is another important factor controlling the polymerization kinetics in the nanoconfinements of the LLCs. To determine the controlling parameter, we performed the same experiments with hexagonal LLC structure to investigate if the same trend is observed for polymerization kinetics.

As shown in Fig. 5, the reaction kinetics in the hexagonal LLC changes in a fashion similar to what is observed for lamellar phase, i.e., the fastest polymerization rate is observed when APS is used. The maximum reaction rate for APS is ~1.6 and ~2.7 times higher than that for AIBN and BPO-initiated samples, respectively. The monomer conversion of about 90% is achieved for APS and AIBN, whereas the conversion of 65% is seen for BPO. Furthermore, similar to the polymerization in lamellar structure, an improvement in the polymerization rate as well as monomer conversion is seen for AIBN+APS and BPO+APS.

Although the overall trends of polymerization kinetics are similar in lamellar and hexagonal structures, some noticeable differences exist in terms of the values of polymerization rates and

monomer conversions. Therefore, it seems crucial to have a comparison between the results for lamellar and hexagonal phases. Since we have normalized the polymerization rate to the monomer concentration, we can compare the polymerization kinetics irrespective of monomer concentration difference between these two LLC structures. Analysis of SAXS data revealed that the nanoconfinement size of 0.5 and 1.2 nm is obtained for lamellar and hexagonal LLCs, respectively. We have shown that as the size of confinement decreases, the local concentration of radicals and macroradicals increases, enhancing the termination reaction and thus slowing down the polymerization in LLCs.[30] Similarly, lower reaction rate and monomer conversion is observed for lamellar structure for BPO- and AIBN-initiated reactions. In APS-initiated systems, however, the polymerization rate and overall monomer conversion is slightly higher for lamellar structure compared to hexagonal counterpart. We hypothesize that since the free radicals of APS are generated in the non-reactive phase and then migrate into the monomer phase, the local concentration of radicals/macroradicals gradually rises in the monomer phase. This phenomenon lowers the chance of termination reactions. In addition, the higher contents of active species near the walls in IFW system can have a similar effect on the polymerization rate as reported for the polymerization in hard templates,[57] in which the template surface acts as a catalyst for initiation, resulting in higher polymerization rate at early stages. When comparing lamellar and hexagonal structures, we note that the different trend in APS initiated system is caused by the competition between (i) gradual increase in radicals/macroradicals initiated from interface and (ii) enhancement of termination reactions due to confinement. In AIBN and BPO initiated systems, only the latter phenomenon is dominant.

Combined APS and AIBN initiators show an improvement in the polymerization rate and double bond conversion in hexagonal structure similar to lamellar phase. The reason for such improvement is that the concentration of free radicals generated by AIBN decreased in half and the other half is gradually provided by APS, resulting in lower termination rate in oil phase. Thus, the chain propagation rate increases in AIBN+APS system. The same improvement is also noticeable for the combination of APS and BPO over IFO polymerization with BPO. Nevertheless, for both BPO and APS+BPO cases, hexagonal structure still exhibits faster polymerization rate as well as higher monomer conversion than the lamellar one. Given the fact that BPO generates less free radicals compared to APS and AIBN (see Fig. S3), enhanced termination reaction is not the only factor affecting the polymerization kinetics initiated by BPO. One phenomenon that might predominate in BPO-initiated system is the recombination of free radicals due to the cage effect in the nanoconfinements of lamellar structure. In other words, under nanoconfinement, the initiator efficiency (f in equation 8; *vide infra*) is much lower for BPO in comparison to other initiators. Bigger size of radicals generated by BPO compared to those by APS and AIBN can be the reason of such difference. Relative immobility of radicals under nanoconfinement increases the chance of their recombination. Similar observation has been reported by Guymon and coworkers for polymerization of LLCs using different photoinitiators.[36] To prove this hypothesis, further tests were required to shed lights on this point.

We evaluate if combining IFO and IFW systems has a synergistic effect on the polymerization rate in LLCs. Table 2 lists the average values of maximum polymerization rate and overall monomer conversion for different initiation system. It also contains the theoretical average values of IFO and IFW systems and compare them with the experimental results for IFW+IFO system. Synergistic effect is evident for the monomer conversion for both lamellar and hexagonal structures as the IFW+IFO systems show higher conversion than the average value of their corresponding single initiation systems. Having a good balance between propagation rate and terminate rate may be the reason why the synergistic effect is observed. In the case of maximum polymerization rate, the synergistic effect is detected only for the combination of APS and AIBN in the lamellar structure.

Table 2. Overall monomer conversion and maximum polymerization rate for different initiation systems and theoretical average values for APS+AIBN and APS+BPO mixtures.

Initiation system	Hexagonal		Lamellar	
	Conversion (%)	$\{R_p / [M]_0\}_{max}$ (min^{-1})	Conversion (%)	$\{R_p / [M]_0\}_{max}$ (min^{-1})
APS	91.4	0.92	95.4	1.00
AIBN	88.1	0.58	74.8	0.37
BPO	65.1	0.34	48.9	0.28
APS+AIBN	93.6	0.71	97.1	0.75
Average of APS and AIBN	89.7	0.75	85.1	0.68
APS+BPO	90.7	0.63	79.2	0.52
Average of APS and BPO	78.2	0.63	72.1	0.64

Based on the obtained results, the gradual increase of propagating chains in monomer phase and thus suppressed termination rate is the main reason why the polymerization rate is faster for IFW than IFO system. To further confirm this hypothesis, we run the same experiments in both LLC structures using initiator concentration of 2.5 mol% with respect to the total monomer content. The results for lamellar phase are presented in Fig. 6a-c. In the unconfined free radical polymerization (e.g., bulk polymerization), the rate of polymerization is proportional to the square root of initiator concentration, meaning that the extent of polymerization (e.g., overall monomer conversion) decreases with a decrease in initiator content.[49] In contrary, we observe an increase in the monomer conversion for all of the initiation systems when the initiator content is reduced to half. This outcome shows that the lower local concentration of macroradicals due to the reduced initiator content is the key factor which determines the rate of termination and thus the extent of the polymerization in LLC nanoconfinements.

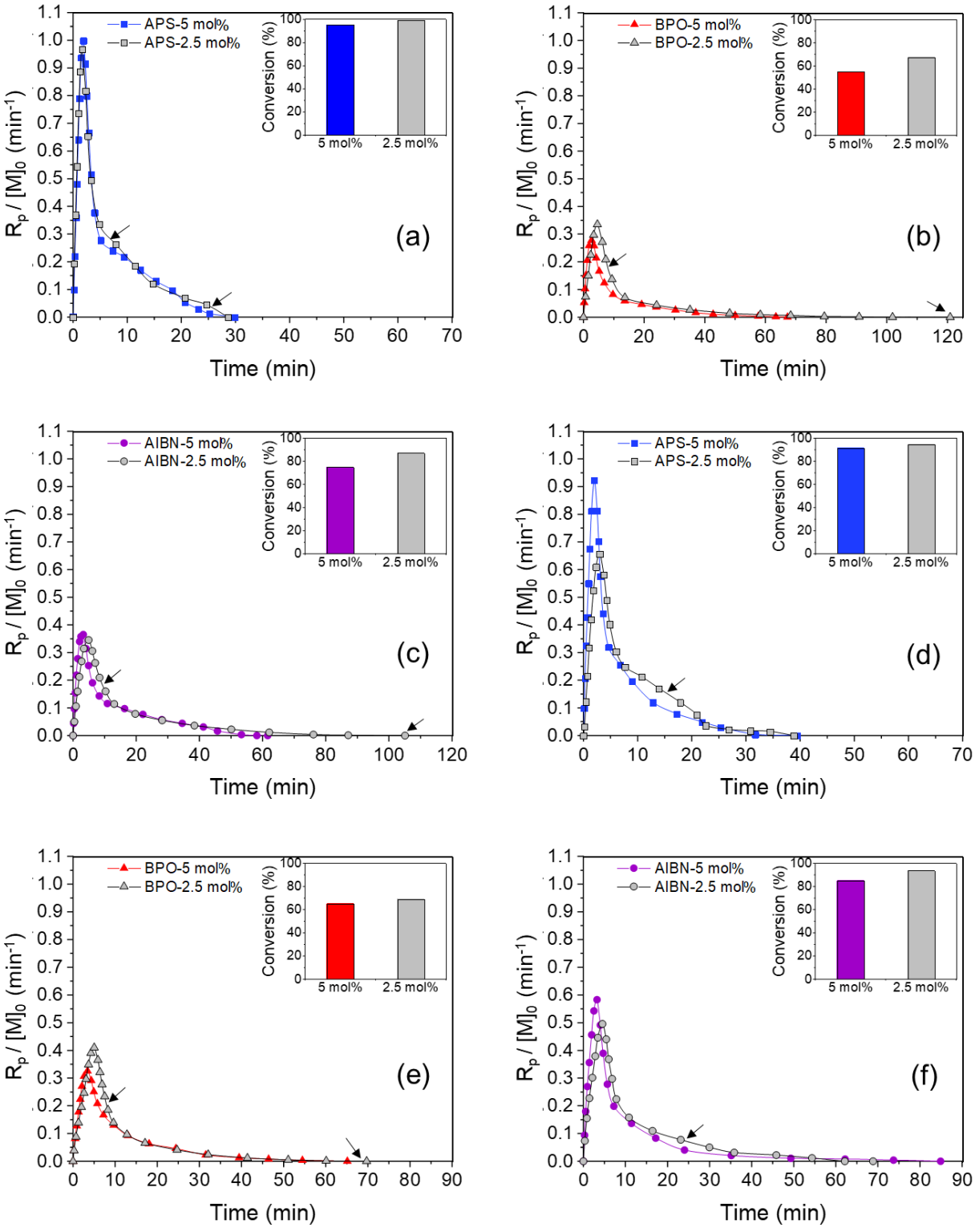

Fig. 6. Normalized polymerization rate versus time and overall monomer conversion obtained from thermal polymerization in (a-c) lamellar and (d-f) hexagonal structures using different initiation systems having varied initiator contents. Arrows denote the time points that show the evidence of reduced termination rate (see main text).

Another important result here is that the maximum reaction rate slightly decreases with a decrease in the initiator content for APS and AIBN, whereas it increases for BPO. At a fixed initiator concentration, the higher the efficiency, the higher the maximum reaction rate will be. Recombination reaction of the free radicals that usually produces nonreactive components is one of the main phenomena that lowers the initiator efficiency. It seems that a portion of free radicals generated by BPO are deactivated through this reaction at high initiator contents due to the relative immobility of radicals. With a decrease in BPO concentration, the proximity of generated free radicals decreases, resulting in lower chance of recombination reactions and therefore higher initiator efficiency. The enhanced initiator efficiency can improve the maximum reaction rate if the number of total initiation sites is increased. This phenomenon is evident only for BPO possibly since it generates fewer free radicals at a given time compared to AIBN (see Fig. S3). Even if we assume that both AIBN and BPO can undergo the recombination of free radicals under confinement in a same fashion, the polymerization rate with BPO will be affected more intensely since it is already vulnerable due to the relative immobility of its radicals. This observation approves our speculation concerning different polymerization kinetics with BPO initiator in LLC structures compared to APS and AIBN.

Similar trend in polymerization rate and monomer conversion is observed in hexagonal structure when the initiator content is decreased to half (Fig. 6d-f). The monomer conversion increases for all of the initiators and the maximum polymerization rate increases for BPO-initiated system, whereas it decreases for AIBN and APS. As discussed for lamellar structure, lower active site concentration due to the decreased initiator content reduces the termination reaction, resulting in higher monomer conversion. The reduced termination rate is evident in the reaction kinetics curves either in the form of an extended time of reaction and/or gradual decrease of the polymerization rate after the peak of the reaction rate as indicated by the arrows in Fig. 6. As mentioned earlier, in the theory of free radical polymerization, the reaction rate scales with the square root of initial initiator concentration, i.e., $R_p \propto ([I]_0)^{0.5}$.[49] The maximum polymerization rate of APS-initiated system in hexagonal structure follows this scaling (Fig. S4), suggesting that other factor(s) (e.g., enhanced recombination of free radicals due to confinement) has negligible effect on the polymerization reaction. Nevertheless, for other cases (e.g., polymerization in lamellar structure with different initiators and reaction in hexagonal phase using AIBN and BPO), this relation is not valid probably due to the occurrence of nanoconfinement-related phenomena such as the recombination of free radicals, diffusion limitations of free radicals, and free radicals concentration gradient in the confinements.

The polymerization temperature is an important factor controlling the reaction kinetics. The kinetics for different initiators were studied using lamellar and hexagonal structures at 55, 65, and 75 °C (Fig. 7). As expected, the maximum polymerization rate increased for all of the initiators when temperature increased. However, the trend of monomer conversion with temperature change was not anticipated. The overall monomer conversion decreases for APS and AIBN-initiated systems when the temperature increases from 65 to 75 °C, which can be due to two main factors.

First, the faster kinetics of cross-linking chains at higher temperatures can expedite the formation of polymer network and thus suppress the mobility of macroradicals. Such effect has already been reported in the literature for the polymerization in LLC structures.[58] Second, the concentration of propagating chains increases sharply in a short period of time with an increase in the temperature, which results in higher local concentration of macroradicals and therefore enhanced termination rate. The simultaneous presence of these two factors reduces the monomer conversion. Nevertheless, the conversion for BPO-initiated polymerization slightly increases with temperature from 65 to 75 °C. The limited local concentration of macroradicals due to the lower free radical concentration generated by BPO (Fig. S3) compared to the other initiators is likely the reason why its double bond conversion does not change in similar fashion to AIBN and APS initiated polymerizations when the temperature increases to 75 °C. In other words, nanoconfinement has less effect on the termination rate at high temperatures in the case of BPO compared to AIBN and APS due to the limited number of free radicals and macroradicals generated by BPO. In addition, BPO is subjected to the cage effect at low polymerization temperatures. Thus, the diminishing cage effect at higher temperatures can be another reason for the difference between BPO and the other initiators. Overall, the results show that the rate of termination reaction and free radical recombination in LLC nanoconfinement control the polymerization rate and monomer conversion.

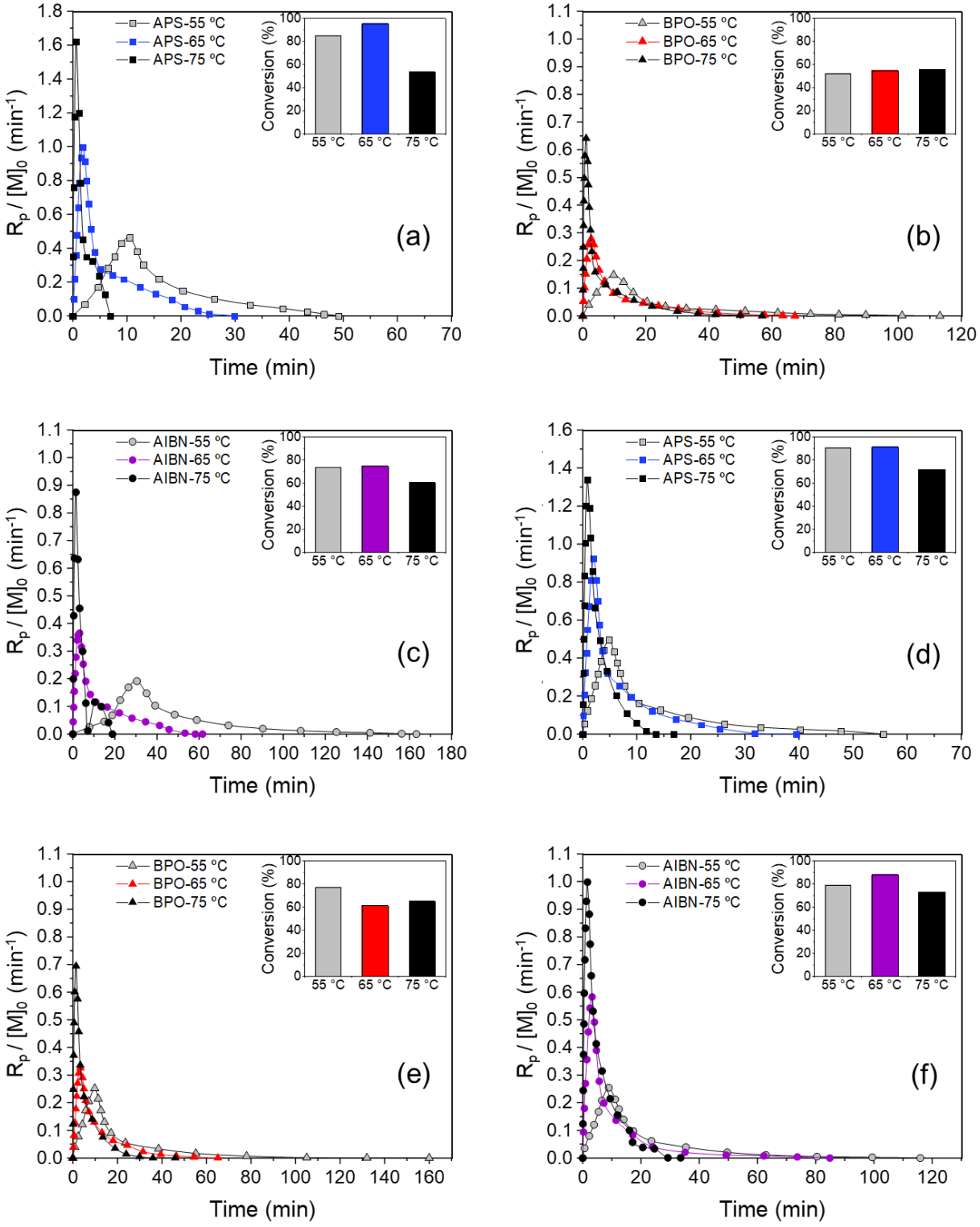

Fig. 7. Normalized polymerization rate versus time and overall monomer conversion obtained from thermal polymerization in (a-c) lamellar and (d-f) hexagonal structures using different initiation systems at varied reaction temperatures. For all samples, the total initiator concentration of 5 mol% was used with respect to the total monomer content.

For IFW system, the polymerization is faster in lamellar structure than hexagonal one (although it has smaller confinement) and opposite behavior is observed for IFO systems at three different temperatures. Similar trend is also seen when different contents of initiators are employed. As a conclusion, for IFW system, polymerization rate is always faster for studied lamellar structure, whereas the reaction rate has higher pace in hexagonal phase for IFO systems. Therefore, the reaction rate in soft nanoconfinement not only depends on the confinement size, but also the loci of polymerization reaction.

To quantify the aforementioned conclusion, we calculated the overall kinetics rate coefficient, K', and the overall activation energy of the polymerization, E. By considering the steady-state hypothesis for the free radical polymerization, normalized polymerization rate can be written as a function of the double bond conversion, X:[59]

$$\frac{R_p(t)}{[M]} = \frac{dX}{dt} = k_p \left(\frac{fk_d}{k_t} \right)^{\frac{1}{2}} [I]^{\frac{1}{2}} (1-X) \cong K'(1-X) \tag{8}$$

$$K' = k_p \left(\frac{fk_d}{k_t} \right)^{\frac{1}{2}} [I]^{\frac{1}{2}} \tag{9}$$

where k_d, k_p, f, k_t, and $[I]$ are kinetics rate constant of initiator decomposition, the propagation rate constant, initiator efficiency, the termination rate constant, and initiator concentration, respectively.

For low degrees of monomer conversion (1% to 10% in the current systems), it is possible to have an expression which directly correlates double bound conversion to the overall polymerization rate coefficient, K':[59]

$$-\ln(1-X) = K't \tag{10}$$

The slope of $-\ln(1-X)$ versus t in conversion range of 1 to 10% gives K'.[59,60] Having the reaction kinetics data at different polymerization temperatures for APS, AIBN and BPO, we calculated the overall activation energy of the polymerization (in both lamellar and hexagonal structures) by considering Arrhenius type dependency of reaction rate to temperature (Table 3). For APS initiator, higher values of K' at different temperatures (Fig. S5) and lower activation energy in lamellar structure compared to hexagonal one confirm the higher reaction rate in lamellar phase. An opposite trend is observed for AIBN and BPO-initiated systems, implying that the reaction rate is higher in hexagonal structure for IFO systems. Additionally, APS shows the lowest activation energy as well as the highest K' values at different temperatures. These results reveal that, under nanoconfinement, APS is the most efficient initiator among the studied initiation systems in terms of polymerization kinetics.

Table 3. Calculated overall kinetics rate coefficient at different temperatures and overall activation energy of the polymerization in lamellar and hexagonal structures using different initiators.

Initiator	Structure	K' (10^{-3}/s) at 55 °C	K' (10^{-3}/s) at 65 °C	K' (10^{-3}/s) at 75 °C	Pre-exponential factor	E (kJ/mol)
APS	L_α	0.75	1.71	3.21	3.56×10^{-11}	69.3
	H_2	0.64	1.54	2.82	2.02×10^{-11}	70.2
AIBN	L_α	0.45	0.97	2.15	3.21×10^{-12}	74.3
	H_2	0.51	1.24	2.37	4.28×10^{-12}	73.8
BPO	L_α	0.29	0.76	1.67	2.12×10^{-13}	81.6
	H_2	0.38	0.83	1.73	7.95×10^{-13}	71.1

Chemorheology and Mechanical Properties

Although chemorheology has been used to study polymerization kinetics for many years,[52,61–63] there have been few reports applying this technique for the reaction in nanoconfinements.[64–66] Recently, Qavi et al. have employed this approach to thoroughly investigate the thermal polymerization kinetics during LLC templating.[30] They observed that the rheological properties of samples show three stages at elevated temperatures: induction, polymerization, and final curing. The polymerization rate obtained by DSC correlated well with the rate of increase of dynamic moduli. Also, the mechanical properties of polymerized LLCs can be obtained from viscoelastic measurements after curing.[16]

Fig. 8 shows the chemorheological behavior during polymerization of lamellar and hexagonal LLC structures by using different initiation systems. In the case of lamellar phase (Fig. 8a-c), the dynamic moduli of the sample increase faster for APS compared to the other initiators, meaning that APS-initiated system has the fastest polymerization rate. Additionally, AIBN induces a higher polymerization rate over BPO. The reaction rate for IFW/IFO systems also lies in between the rates for IFW and IFO systems. The interesting result here is that the final values of the moduli for APS-cured sample is higher than other cases. To further examine such difference in mechanical properties, we run frequency sweep experiments on the polymerized samples in less than 2 min after reaching the final curing stage during chemorheological measurements (Fig. 9a). The results indicate higher dynamic moduli for APS-cured sample. One may argue that this is due to the higher monomer conversion of APS initiated sample compared to IFO systems. Based on the DSC results, however, the double bond conversion for APS/AIBN system is almost equal to that for APS alone, but it has lower dynamic moduli than that of APS system. Therefore, there should be an additional parameter affecting the mechanical properties of the samples. Investigating the results gained for hexagonal structure can shed lights on this point.

Chemorheology study on hexagonal structure not only shows that the polymerization rate is faster for APS compared to other initiators, but also reveals an unexpected phenomenon in the

development of dynamic moduli during reaction with APS (Fig. 8d-f). When APS is used (in the pure form or in combination with other initiators), the storage (G') and loss moduli (G") increase sharply and then decrease to some extent followed by a partial recovery. Such change in mechanical properties during polymerization, which is seen only for APS-initiated reactions, is probably due to the way that free radicals migrate from water to the monomer phase. In emulsion polymerization, as a generally accepted mechanism, the free radicals located in aqueous phase first react with monomer molecules dissolved (even in very low concentrations) in the aqueous phase to form surface active species (called z-mers) that subsequently enter the monomer droplets.[67,68] When APS is used in polymerization of LLCs, the z-mers probably form and either remain at the interface or enter the oil phase to react with the large reservoir of monomers. Since the oil/water interface is mechanically the weakest component in multiphase systems, the propagation of polymer chains at the interface results in a sharp increase in the moduli. However, detachment of growing z-mers from the interface and their entrance into the monomer phase may induce a decline in moduli. Further propagation and formation of polymer network results in a recovery of the mechanical properties to some extent. We speculate that the formation of a robust polar/apolar interface in IFW system is one of the reasons of higher mechanical strengths of the cured samples compared to IFO ones in different LLC structures, as shown in Fig. 9. It is worth noting that we do not see the peak in dynamic moduli during the reaction in lamellar phase (see Fig. 8a-c) in contrast to hexagonal structure. This can be due to the structure itself and/or lower monomer content in lamellar phase.

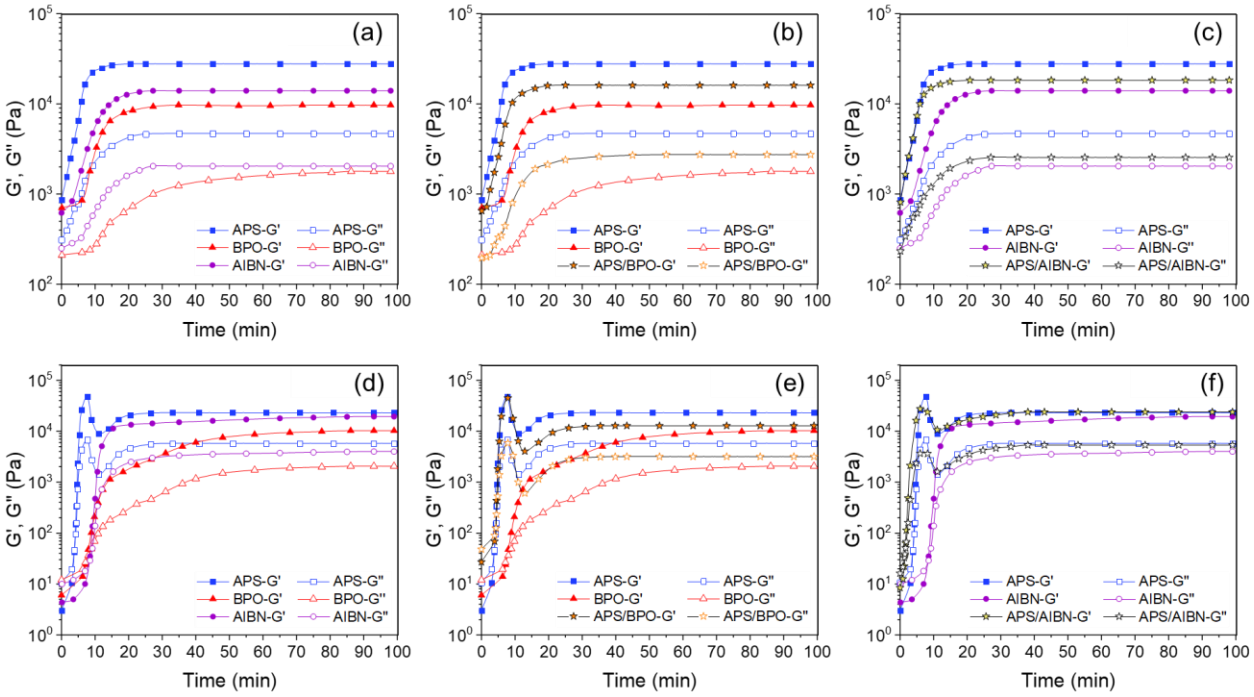

Fig. 8. Evolution of dynamic moduli during LLC templating with (a-c) lamellar and (d-f) hexagonal structures using different initiation systems.

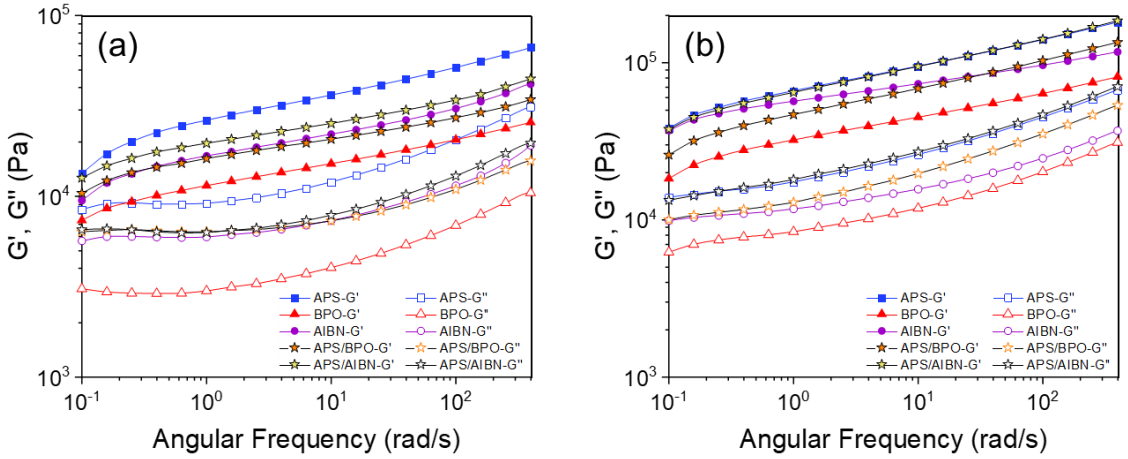

Fig. 9. Frequency sweep curves of the samples obtained from polymerization in (a) lamellar and (b) hexagonal LLC structures using different initiation systems.

To further examine the effect of initiation system on the mechanical properties of the polymerized samples, we conduct rheological measurements on the LLCs containing 2.5 mol% initiator content, which have less termination reaction than 5 mol% samples as discussed earlier. The samples containing 2.5 mol% APS and AIBN are used in this part as they show almost similar monomer conversion according to DSC analysis. The results are presented in Fig. 10. For both initiation systems, the dynamic moduli of the polymerized samples having different nanostructures are enhanced with a decrease in the initiator content. Furthermore, APS-cured samples exhibit higher moduli over the samples cured with AIBN even under almost same monomer conversions. These observations confirm the considerable effect of the chains forming at the interface on the mechanical properties of polymerized LLCs. To further elaborate the effect of the chains formed at the water/oil interface, we have schematically presented the probable mechanism (as discussed above) in Fig. 11. In summary, free radicals generated by the water-soluble initiator migrate to the polar/apolar interface and start the polymerization, resulting in the formation of z-mers. The growing z-mers can either continue the reaction at the interface or detach from the interface to continue the polymerization in the apolar domain. A robust polar/apolar interface is obtained at the end of the reaction due to the formation of polymer chains at the interface resulting in an enhanced mechanical properties. In the case of IFO system, however, the polymerization mainly takes place in monomer phase. Such polymerization behavior limits the reaction at the interface, resulting in the formation of less polymer chains in this location and thus acquiring weaker mechanical properties compared to IFW system.

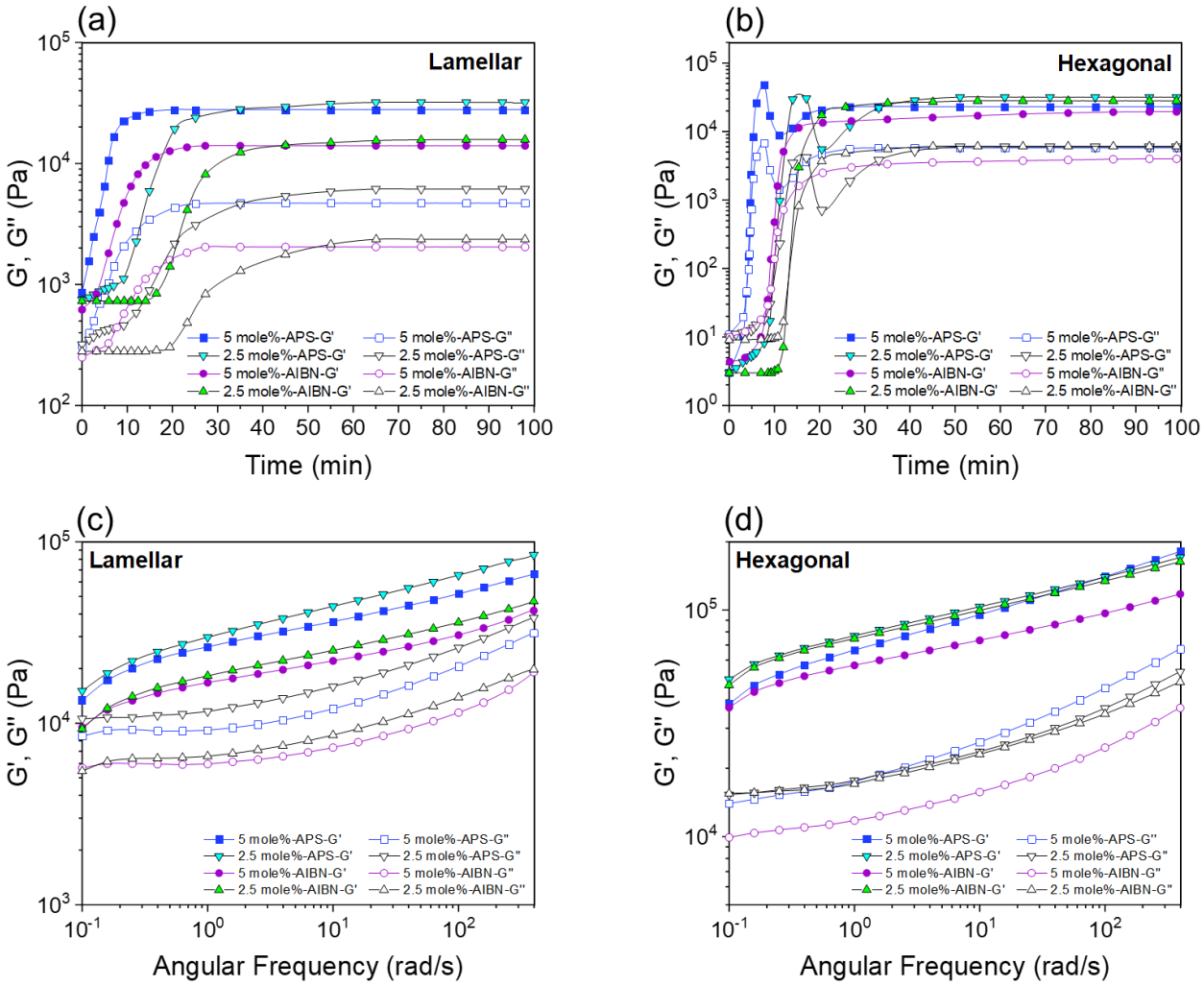

Fig. 10. (a, b) Evolution of dynamic moduli during LLC templating and (c, d) frequency sweep curves of polymerized LLCs using different initiator contents.

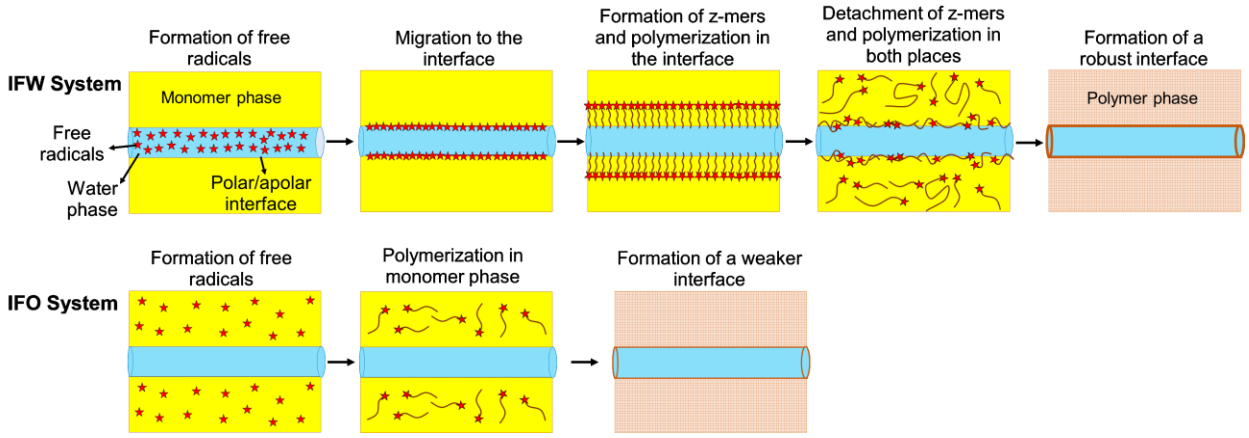

Fig. 11. Schematic diagram of the polymerization mechanism in IFW and IFO systems and the consequent difference in the robustness of the polymerized LLCs.

Conclusion

Different thermal initiators were used to study the polymerization kinetics in lamellar and reverse hexagonal LLC structures through DSC analysis. The IFW system showed a faster polymerization rates over IFO ones under any circumstances (e.g., different temperature, initiator concentration, and LLC structure). We attributed this behavior to the gradual increase of the propagating chains in the monomer phase which results in lower termination rate and thus higher overall polymerization rate. Moreover, the experimental results showed that the polymerization rate in lamellar phase is faster than in hexagonal phase when IFW system is used, whereas an opposite trend is observed for IFO systems. Additionally, rheological measurements not only confirmed the DSC results concerning the faster reaction rates by IFW system, but also revealed that the samples cured by IFW system exhibit enhanced mechanical strength over other initiation systems even at similar monomer conversions. We attributed this observation to the polymerization at polar/apolar interface in IFW system.

Acknowledgements

This work was supported by the National Science Foundation under grant no. 1840871. Parts of this work was performed at the Center for Integrated Nanotechnologies, an Office of Science User Facility operated for the U.S. Department of Energy (DOE) Office of Science. Los Alamos National Laboratory, an affirmative action equal opportunity employer, is managed by Triad National Security, LLC for the U.S. DOE's NNSA under contract 89233218CNA000001.

Conflict of interest

The authors declare no conflict of interest.

References

1 D. Chimene, D. L. Alge and A. K. Gaharwar, *Adv. Mater.*, 2015, **27**, 7261–7284.

2 N. M. Bardhan, *J. Mater. Res.*, 2017, **32**, 107–127.

3 J. R. Werber, C. O. Osuji and M. Elimelech, *Nat. Rev. Mater.*, 2016, **1**, 16018.

4 D. Wandera, S. R. Wickramasinghe and S. M. Husson, *J. Memb. Sci.*, 2010, **357**, 6–35.

5 Q. Zhang, E. Uchaker, S. L. Candelaria and G. Cao, *Chem. Soc. Rev.*, 2013, **42**, 3127–3171.

6 D. L. Gin, X. Lu, P. R. Nemade, C. S. Pecinovsky, Y. Xu and M. Zhou, *Adv. Funct. Mater.*, 2006, **16**, 865–878.

7 H. Hu, M. Gopinadhan and C. O. Osuji, *Soft Matter*, 2014, 10, 3867–3889.

8 Y. Xie, R. Xie, H. C. Yang, Z. Chen, J. Hou, C. R. López-Barrón, N. J. Wagner and K. Z. Gao, *ACS Appl. Mater. Interfaces*, 2018, **10**, 32435–32443.

9 R. L. Kerr, S. A. Miller, R. K. Shoemaker, B. J. Elliott and D. L. Gin, *J. Am. Chem. Soc.*, 2009, **131**, 15972–15973.

10 S. M. Dischinger, J. Rosenblum, R. D. Noble, D. L. Gin and K. G. Linden, *J. Memb. Sci.*, 2017, **543**, 319–327.

11 X. Feng, Q. Imran, Y. Zhang, L. Sixdenier, X. Lu, G. Kaufman, U. Gabinet, K. Kawabata, M. Elimelech and C. O. Osuji, *Sci. Adv.*, 2019, **5**, eaav9308.

12 B. S. Forney, C. Baguenard and C. Allan Guymon, *Soft Matter*, 2013, **9**, 7458–7467.

13 J. D. Clapper and C. A. Guymon, *Macromolecules*, 2007, **40**, 7951–7959.

14 S. T. Hyde, in *Handbook of Applied Surface and Colloid Chemistry*, 2001, pp. 299–332.

15 K. S. Worthington, C. Baguenard, B. S. Forney and C. A. Guymon, *J. Polym. Sci. Part B Polym. Phys.*, 2017, **55**, 471–489.

16 A. Bandegi, J. L. Bañuelos and R. Foudazi, *Soft Matter*, 2020, **16**, 6102–6114.

17 D. L. Gin, W. Gu, B. A. Pindzola and W. J. Zhou, *Acc. Chem. Res.*, 2001, **34**, 973–980.

18 J. D. Clapper, S. L. Iverson and C. A. Guymon, *Biomacromolecules*, 2007, **8**, 2104–2111.

19 J. R. McLaughlin, N. L. Abbott and C. A. Guymon, *Polymer*, 2018, **142**, 119–126.

20 D. L. Gin, J. E. Bara, R. D. Noble and B. J. Elliott, *Macromol. Rapid Commun.*, 2008, **29**, 367–389.

21 H.-P. Hentze, C. C. Co, C. A. McKelvey and E. W. Kaler, in *Topics in Current Chemistry*, 2003, pp. 197–223.

22 P. Ström and D. M. Anderson, *Langmuir*, 1992, **8**, 691–709.

23 J. Zhang, Z. A. Qiao, S. M. Mahurin, X. Jiang, S. H. Chai, H. Lu, K. Nelson and S. Dai, *Angew. Chemie - Int. Ed.*, 2015, **54**, 4582–4586.

24 S. Qavi, A. P. Lindsay, M. A. Firestone and R. Foudazi, *J. Memb. Sci.*, 2019, **580**, 125–133.

25 M. Zhou, P. R. Nemade, X. Lu, X. Zeng, E. S. Hatakeyama, R. D. Noble and D. L. Gin, *J. Am. Chem. Soc.*, 2007, **129**, 9574–9575.

26 D. T. McCormick, K. D. Stovall and C. A. Guymon, *Macromolecules*, 2003, **36**, 6549–

6558.

27 C. Liang and S. Dai, *J. Am. Chem. Soc.*, 2006, **128**, 5316–5317.

28 C. M. Ghimbeu, M. Sopronyi, F. Sima, C. Vaulot, L. Vidal, J. M. Le Meins and L. Delmotte, *RSC Adv.*, 2015, **5**, 2861–2868.

29 S. Herou, M. C. Ribadeneyra, R. Madhu, V. Araullo-Peters, A. Jensen, P. Schlee and M. Titirici, *Green Chem.*, 2019, **21**, 550–559.

30 S. Qavi, A. Bandegi, M. Firestone and R. Foudazi, *Soft Matter*, 2019, **15**, 8238–8250.

31 L. Sievens-Figueroa and C. A. Guymon, *Macromolecules*, 2009, **42**, 9243–9250.

32 C. L. Lester and C. A. Guymon, *Polymer*, 2002, **43**, 3707–3715.

33 L. Sievens-Figueroa and C. Allan Guymon, *Polymer*, 2008, **49**, 2260–2267.

34 C. L. Lester, C. D. Colson and C. A. Guymon, *Macromolecules*, 2001, **34**, 4430–4438.

35 M. A. DePierro, A. J. Olson and C. A. Guymon, *Radtech Tech. Proc.*, 2004.

36 M. A. DePierro, A. J. Olson and C. A. Guymon, *Polymer*, 2005, **46**, 335–345.

37 M. A. DePierro and C. A. Guymon, *Macromolecules*, 2006, **39**, 617–626.

38 B. S. Forney and C. A. Guymon, *Macromolecules*, 2010, **43**, 8502–8510.

39 C. A. Guymon and C. L. Lester, *ACS Symp. Ser.*, 2003, **847**, 378–388.

40 C. L. Lester, S. M. Smith, W. L. Jarrett and C. Allan Guymon, *Langmuir*, 2003, **19**, 9466–9472.

41 C. L. Lester, S. M. Smith, C. D. Colson and C. A. Guymon, *Chem. Mater.*, 2003, **15**, 3376–3384.

42 C. L. Lester, S. M. Smith and C. A. Guymon, *Macromolecules*, 2001, **34**, 8587–8589.

43 M. A. DePierro, C. Baguenard and C. Allan Guymon, *J. Polym. Sci. Part A Polym. Chem.*, 2016, **54**, 144–154.

44 L. Sievens-Figueroa and C. A. Guymon, *Chem. Mater.*, 2009, **21**, 1060–1068.

45 M. A. DePierro, K. G. Carpenter and C. A. Guymon, *Chem. Mater.*, 2006, **18**, 5609–5617.

46 B. S. Forney, C. Baguenard and C. A. Guymon, *Chem. Mater.*, 2013, **25**, 2950–2960.

47 I. Capek, *Polym. J.*, 2004, **36**, 793–803.

48 P. Alexandridis, U. Olsson and B. Lindman, *Macromolecules*, 1995, **28**, 7700–7710.

49 G. Odian, in *Principles of Polymerization*, John Wiley & Sons, Inc., Hoboken, NJ, USA, 2004.

50 M. A. Depierro and C. A. Guymon, *Macromolecules*, 2014, **47**, 5728–5738.

51 S. Qavi and R. Foudazi, *Rheol. Acta*, 2019, **58**, 483–498.

52 R. Foudazi, P. Gokun, D. L. Feke, S. J. Rowan and I. Manas-Zloczower, *Macromolecules*, 2013, **46**, 5393–5396.

53 C. S. Pecinovsky, E. S. Hatakeyama and D. L. Gin, *Adv. Mater.*, 2008, **20**, 174–178.

54 S. Qavi, M. A. Firestone and R. Foudazi, *Soft Matter*, 2019, **15**, 5626–5637.

55 K. Mortensen, W. Brown and E. Jørgensen, *Macromolecules*, 1995, **28**, 1458–1463.

56 M. Seo and M. A. Hillmyer, *Science (80-.).*, 2012, **336**, 1422–1425.

57 B. Sanz, N. Ballard, J. M. Asua and C. Mijangos, *Macromolecules*, 2017, **50**, 811–821.

58 M. Li, W. Yang, Z. Chen, J. Qian, C. Wang and S. Fu, *J. Polym. Sci. Part A Polym. Chem.*, 2006, **44**, 5887–5897.

59 D. S. Achilias, *J. Therm. Anal. Calorim.*, 2014, **116**, 1379–1386.

60 H. Zhao and S. L. Simon, *Polymer*, 2011, **52**, 4093–4098.

61 B. Strachota, L. Matějka, A. Sikora, J. Spěváček, R. Konefał, A. Zhigunov and M. Šlouf, *Soft Matter*, 2017, **13**, 1244–1256.

62 C. A., S. K., S.-M. J. F. A., W. Q., P. J. A. D. and M.-M. J., *RSC Adv.*, 2016, **6**, 81694–81702.

63 M. Di Biase, P. de Leonardis, V. Castelletto, I. W. Hamley, B. Derby and N. Tirelli, *Soft Matter*, 2011, **7**, 4928.

64 S. Peng, P. G. Hartley, T. C. Hughes and Q. Guo, *Soft Matter*, 2015, **11**, 6318–6326.

65 A. W. Chow, J. F. Sandell and J. F. Wolfe, *Polymer*, 1988, **29**, 1307–1312.

66 A. W. Chow, R. D. Hamlin, J. F. Sandell and J. F. Wolfe, *MRS Proc.*, 1988, **134**, 95.

67 S. C. Thickett and R. G. Gilbert, *Polymer*, 2007, **48**, 6965–6991.

68 I. A. Maxwell, B. R. Morrison, D. H. Napper and R. G. Gilbert, *Macromolecules*, 1991, **24**, 1629–1640.

Graphical abstract